CO/H2 ABUNDANCE RATIO ≈ 10–4 IN A PROTOPLANETARY DISK
France et al., ApJ

目的：円盤でのCO/H2 ratio を求めたい

手法：HSTのCosmic Origins Spectrograph(COS)を使ってfar-UVでH2, COを観測する

今回の天体：RW Aur (K型原始星の連星, primary: 1.1-1.4Msun, secondary: 30-50%重い)

　近赤超過から円盤はあると思われていて円盤質量は電波で4×10^(-3)Msun

今回の観測：HST, 波長帯は1064–1130 Å, resolutionはR>10^4 (=波長分解能0.1Å以下)

結果：

中心星付近の降着領域、円盤、アウトフローという多成分でできていそう(速度で分離)

モデリングの結果、基本的に円盤上層部からの放射である。

この円盤表層（暖かい）では、H2の面密度は19.9 cm^-2 (Trot=440K),molecular fraction >0.47 COの面密度は16.1 cm^-2 (Trot=440K)

fractional abundance: CO/H2 = 1.6 * 10^-4 : 星間物質とほとんど同じ

→余り化学変化がおきていない？(warm layerでは)

Table 3
RW Aur A Disk Abundance Ratios[a]

Species	$\log_{10}N(\mathrm{X})$	$N(\mathrm{X})/N(\mathrm{H_{total}})$[a]
H I	$<20.25^{+0.05}_{-0.21}$	<0.53
H_2	$19.90^{+0.33}_{-0.22}$	>0.24
CO	$16.1^{+0.3}_{-0.5}$	$>3.7 \times 10^{-5}$

Notes.
[a] The majority of the neutral atomic hydrogen on the RW Aur A sightline is thought to be interstellar (McJunkin et al. 2014), therefore relative abundance ratios are lower limits.
[b] $N(\mathrm{H_{total}}) = N(\mathrm{H\,I}) + 2N(\mathrm{H_2})$.

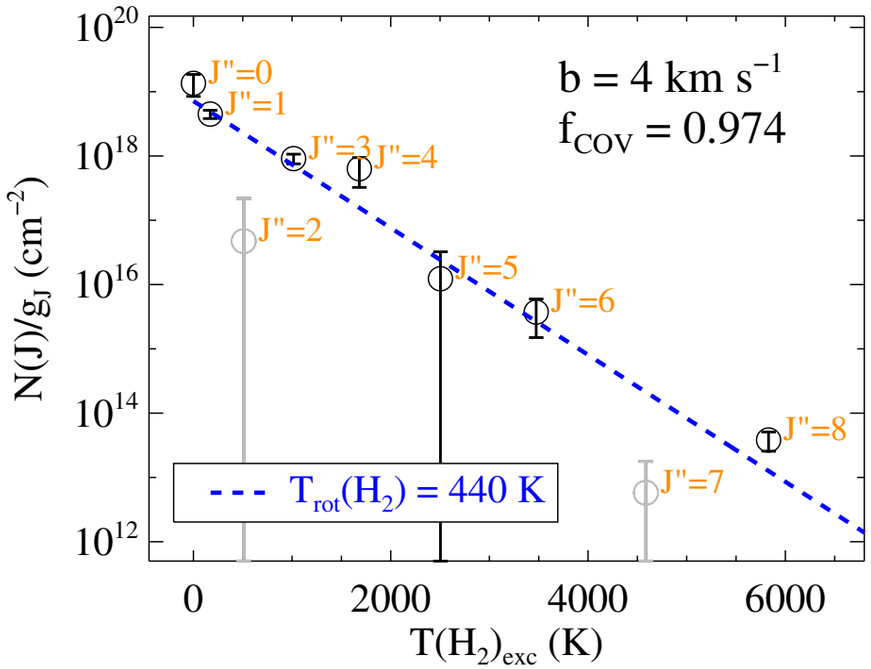

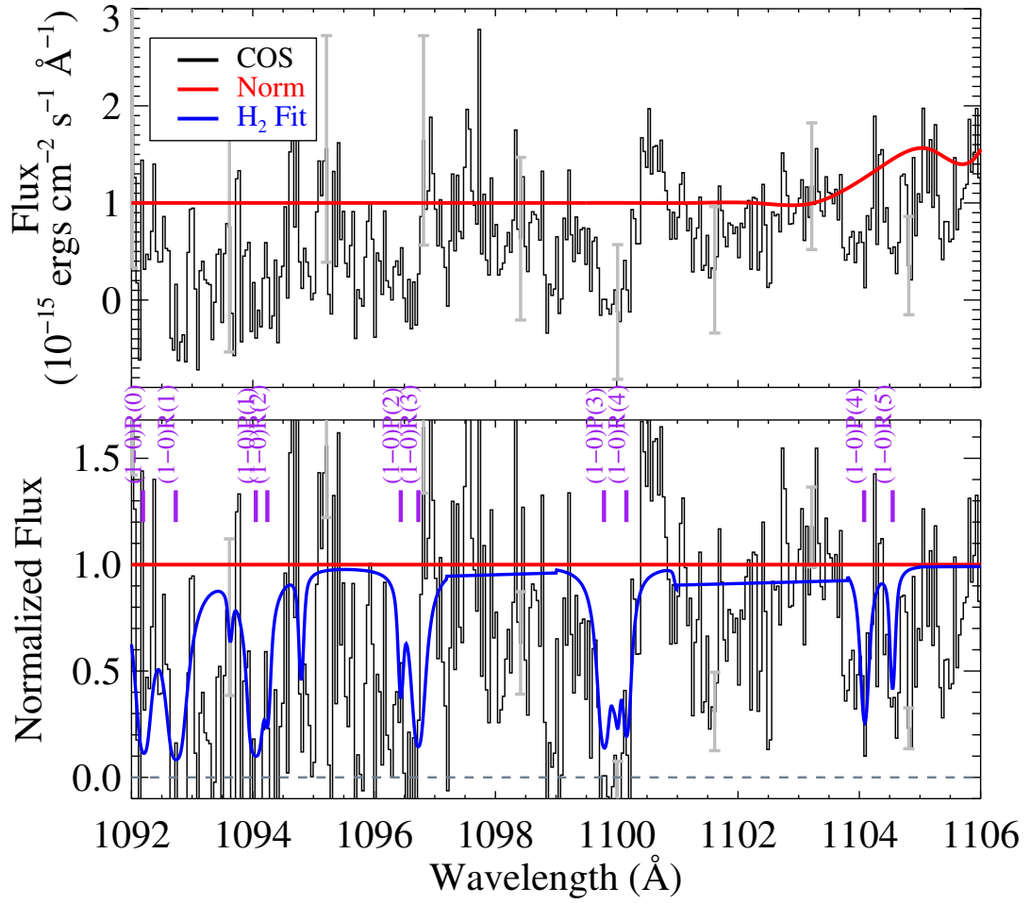

Figure 2. *HST*-COS spectra of the 1092–1106 Å spectral region, with the continuum function shown as the solid red line (top panel). The bottom panel shows the normalized flux and the best-fit H_2 absorption model as the blue solid line (Section 4.1). The strongest H_2 absorption lines with $J'' \leqslant 5$ are labeled in purple. The data and the normalized spectra are binned by 4 pixels and smoothed with a 3 pixel boxcar average for display. The normalized spectra are smoothed with a 3 pixel boxcar average prior to H_2 fitting.

Constraints on photoevaporation models from (lack of) radio emission in the Corona Australis protoplanetary disks⋆

Galvan-Madrid et al., A&A

VLA3.5cmで円盤をたくさん観測した。その結果、10天体中7つでnon-detection

→EUV photonの数に制限をつけた（EUV→電離→free freeが出るはずだから）

→$\Phi_{EUV} < 1–4 \times 10^{41}$ s^{-1}
→これはかなり強い制限。

観測結果+モデル計算

(freefree放射∝EUV)

Table 1. Disks in CrA within the VLA primary beam.

(1) Name	(2) RA [h:m:s]	(3) Dec [deg:arcmin:arcsec]	(4) CSA11	(5) SA13	(6) $S_{3.5\,cm}$ [μJy]	(7) PB-corrected noise [μJy]	(8) L_X [erg s^{-1}]	(9) Spectral type	(10) Comments
G-95	19:01:28.72	–36:59:31.7	TD	...	<180	60	1.03×10^{30}	M1	...
G-87	19:01:32.32	–36:58:03.0	TD	TD	<60	20	...	M1.5	...
G-85	19:01:33.85	–36:57:44.8	PD	pre-TD	<60	20	4.28×10^{29}	M0.5	...
V709	19:01:34.84	–37:00:56.7	TD/DD	...	892 ± 79	50	4.17×10^{30}	K1	a
HBC-677	19:01:41.62	–36:59:53.1	PD	PD	<45	15	2.21×10^{29}	M2	...
IRS8	19:01:51.11	–36:54:12.5	PD	...	<120	40	...	M2	...
R CrA	19:01:53.67	–36:57:08.3	PD	...	285 ± 10	10	7.7×10^{29}	A5	b
CrA-465	19:01:53.74	–37:00:33.9	PD	...	<60	20	...	M5-M7.5	...
G-32	19:01:58.33	–37:00:26.7	PD	...	<60	20	...	>M5	...
T CrA	19:01:58.79	–36:57:50.1	PD	PD	181 ± 9	15	...	F0	c

Notes. Columns 1 to 3: names and coordinates from CSA11 (who use the *Chandra* positions of Forbrich & Preibisch 2007) and SA13. Columns 4 and 5: classification in CSA11 and SA13. Primordial disk (PD), pre-transitional disk (pre-TD), transitional disk (TD), debris disk (DD). A blank field means that the source is either not detected or not mentioned, or that the photometry was affected by extended nebulosity, mostly an issue in the *Herschel* observations (SA13). Column 6: flux density at 3.5 cm or 3σ upper limits. For the detections, the VLA coordinates from Gaussian fits are given as a comment, together with the estimation of the 3.5 cm flux due to free-free emission from the coadded nondetection epochs. Column 7: primary-beam-corrected noise, measured individually around the position of each source. Column 8: X-ray luminosity in the 0.2–8 keV band from Forbrich & Preibisch (2007). A blank field means that only $\sim 10^1$ counts were detected, and the X-ray spectral shape and luminosity could not be derived. However, under typical assumptions, their measured count number would imply $L_X \sim 1 \times 10^{29}$ erg s^{-1}. Column 9: spectral types reported by CSA11. Compiled from Forbrich & Preibisch (2007), Meyer & Wilking (2009), López Martí et al. (2005), and CSA11. Column 10: comments. a) RA = 19:01:34.86, Dec = –37:00.55.8. $S_{V709,ff} \lesssim 507 \pm 88$ μJy. b) RA = 19:01:53.68, Dec = –36:57:08.0. $S_{RCrA,ff} \lesssim 183 \pm 20$ μJy. Intermediate-mass YSO (Acke & van den Ancker 2004). c) RA = 19:01:58.79, Dec = –36:57:49.9. $S_{TCrA,ff} \lesssim 170 \pm 26$ μJy. Intermediate-mass YSO (Acke & van den Ancker 2004).

Name	$\Phi_{EUV,model}$ [s^{-1}]
G-95	$<4.0 \times 10^{41}$
G-87	$<1.3 \times 10^{41}$
G-85	$<1.3 \times 10^{41}$
V709	$\lesssim 1.1 \times 10^{42}$
HBC-677	$<1.0 \times 10^{41}$
IRS 8	$<2.7 \times 10^{41}$
R CrA	$\lesssim 4.1 \times 10^{41}$
CrA-465	$<1.3 \times 10^{41}$
G-32	$<1.3 \times 10^{41}$
T CrA	$\lesssim 3.8 \times 10^{41}$

Astrometric follow-up observations of directly imaged sub-stellar companions to young stars and brown dwarfs*

Ginski et al., MNRAS

＊アブストのみ

6つの星の伴星に対して、アストロメトリーを行った。

軌道要素をモンテカルロ法で制限

特にGQ Lupではseparation と position angleが両方変わった

　エキセントリック or 傾いた円軌道

更にもう一点検出した（かも）

On the filtering and processing of dust by planetesimals
1. Derivation of collision probabilities for non-drifting planetesimals
Guillot et al., A&A

円盤内の固体はダスト(ミクロン~cm~)から微惑星までサイズが多岐にわたる。

大きなダスト(mm~m)は動径方向に落ちていく

もし、微惑星(km)が漂っていたら、落ちていく大きなダストは微惑星と衝突合体するだろうか？

この論文：ダストが微惑星に衝突する確率を導出・定式化

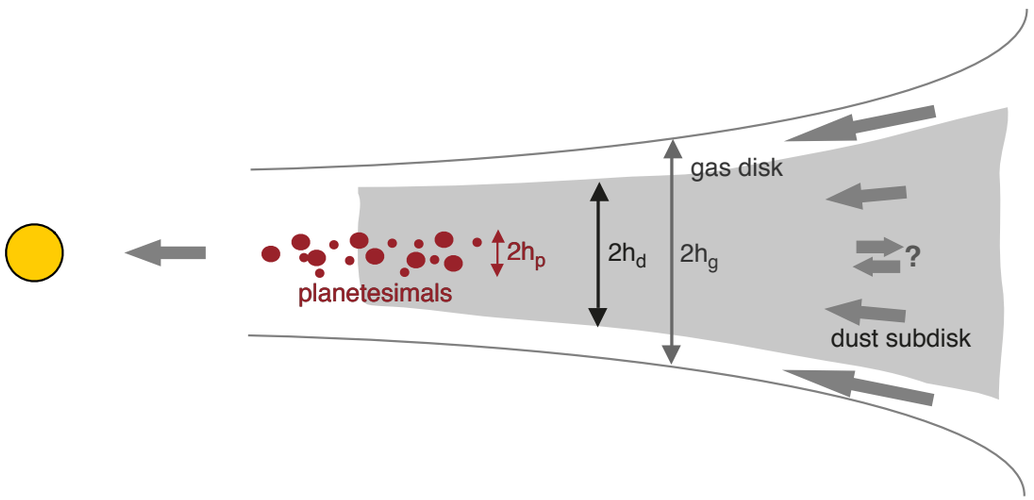

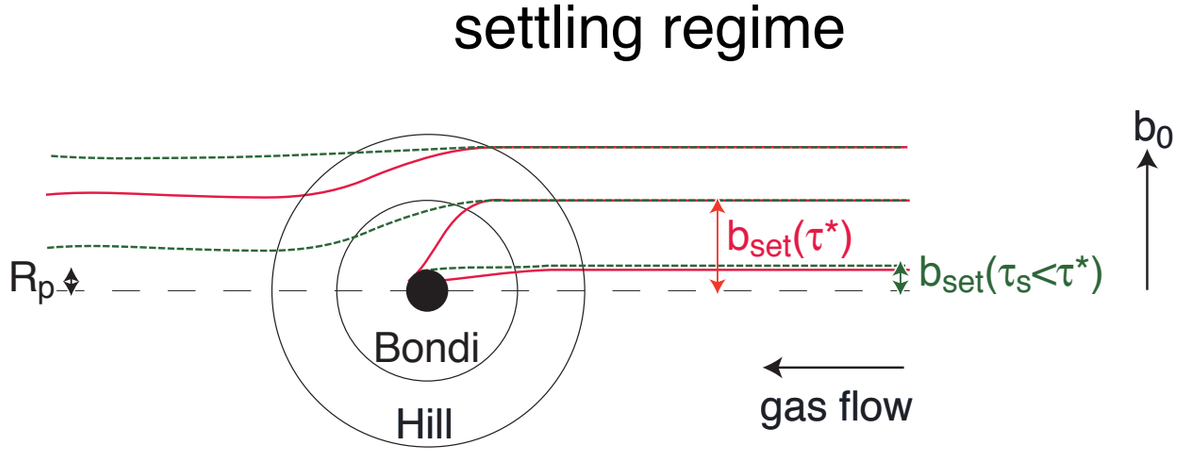

Fig. 8. Illustration of dust capture in the settling regime. Planetesimals with a radius R_p between about 100 km and 1000 km have a Bondi radius larger than R_p but smaller than the Hill radius (see text). For the critical stopping time τ_s^* corresponding to a stopping time equal to the time necessary for the unperturbed dust particle to cross the Bondi sphere, the effective cross section for capture is $b_\mathrm{set} \sim R_\mathrm{B}$. The approximate trajectory of the dust for $\tau_\mathrm{s} = \tau_\mathrm{s}^*$ is indicated by red lines. For smaller dust particles with $\tau_\mathrm{s} < \tau_\mathrm{s}^*$ (dashed green lines), the deflection by the gravitational pull of the planetesimal is smaller, hence a smaller effective capture radius.

設定：

微惑星が0.1AU-35AUに分布しているとする

$$X_{\rm filter}(s) \equiv \int_{r_{\rm in}}^{r_{\rm out}} \frac{d}{dr}\left(\int_{R_{\rm p,min}}^{R_{\rm p,max}} \mathcal{P}\frac{dN_{\rm p}}{dR_{\rm p}}dR_{\rm p}\right)dr.$$

Xfilter>1 ⇒効率よく微惑星に食べられる

結果:

乱流が典型的な値の場合(α=10^-2)、filtering efficiency は低い（ダストは微惑星にあまり衝突せず、中心星に落下していく。

乱流が弱い場合(α=10^-4)、微惑星サイズに依存してfilteringが変わる

1)微惑星が10kmよりも小さい時

幾何断面積での衝突

filtering efficiency $\propto r^{-7/4}$

2)微惑星(原始惑星)が1000kmより大きく、そのスケールハイトがガスの1/10以下で、かつダストがmmより大きい時、

沈殿regimeで衝突

filtering efficiency $\propto r^{-1/4} \sim r^{1/4}$

応用例：例えば、地球付近が水浸しにならないのは、氷ダストが途中で微惑星に食べられたから？→だとすると、弱い乱流モデルがfavorされる

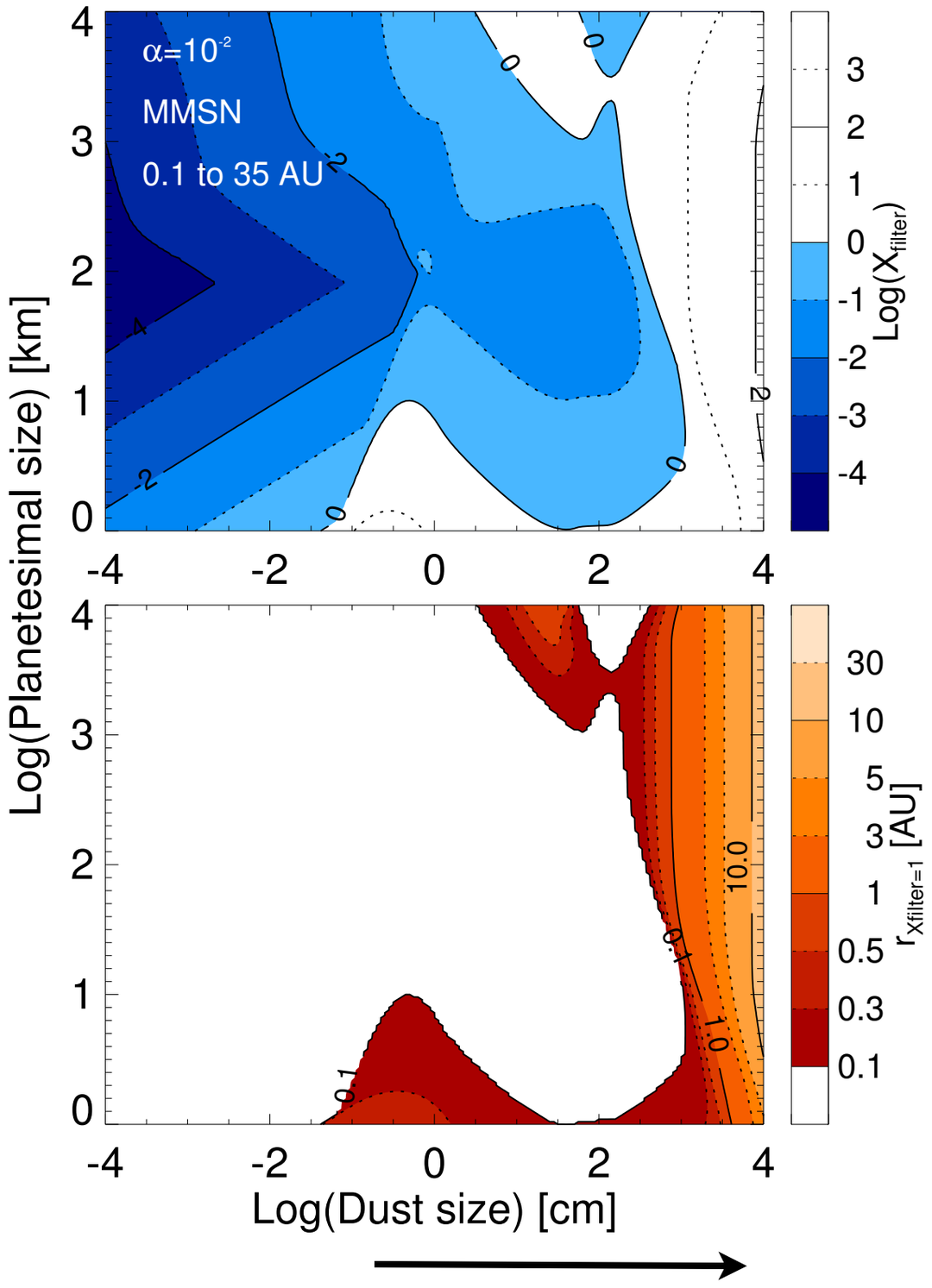

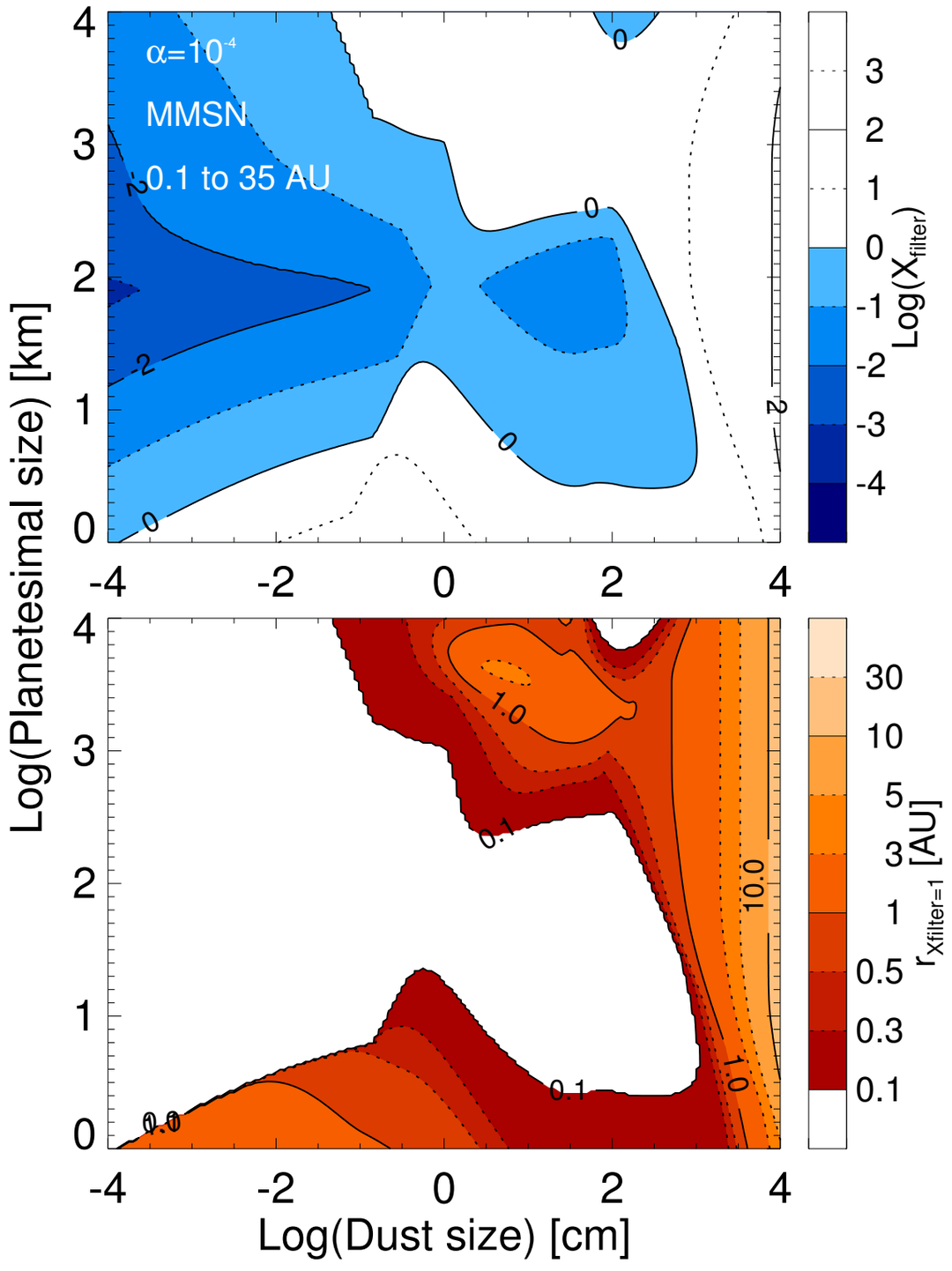

ダストが大きくないとfilterされない

0.1-1AUというとても内側

Slow ionized wind and rotating disklike system associated with the high-mass young stellar object G345.4938+01.4677
Guzman et al., ApJ

ALMA 85-99GHzの連続波で、大質量星形成クランプIRAS16562–3959を観測

中に大質量YSOのG345.49+1.47. (~15Msun)がある。ionized windがふいている

1.7kpc, cluster: ~900Msun

結果：

H40α, H42α, H50β の水素再結合線を検出。

低速アウトフローモデルで結果を再現した。

Lorentzian wingから電子密度を求めると5×10^7 cm^{-3}

SOとSO_2も検出(~3000AU)：回転構造も検出

→遅い電離ウインドを伴った大質量原始星の描像

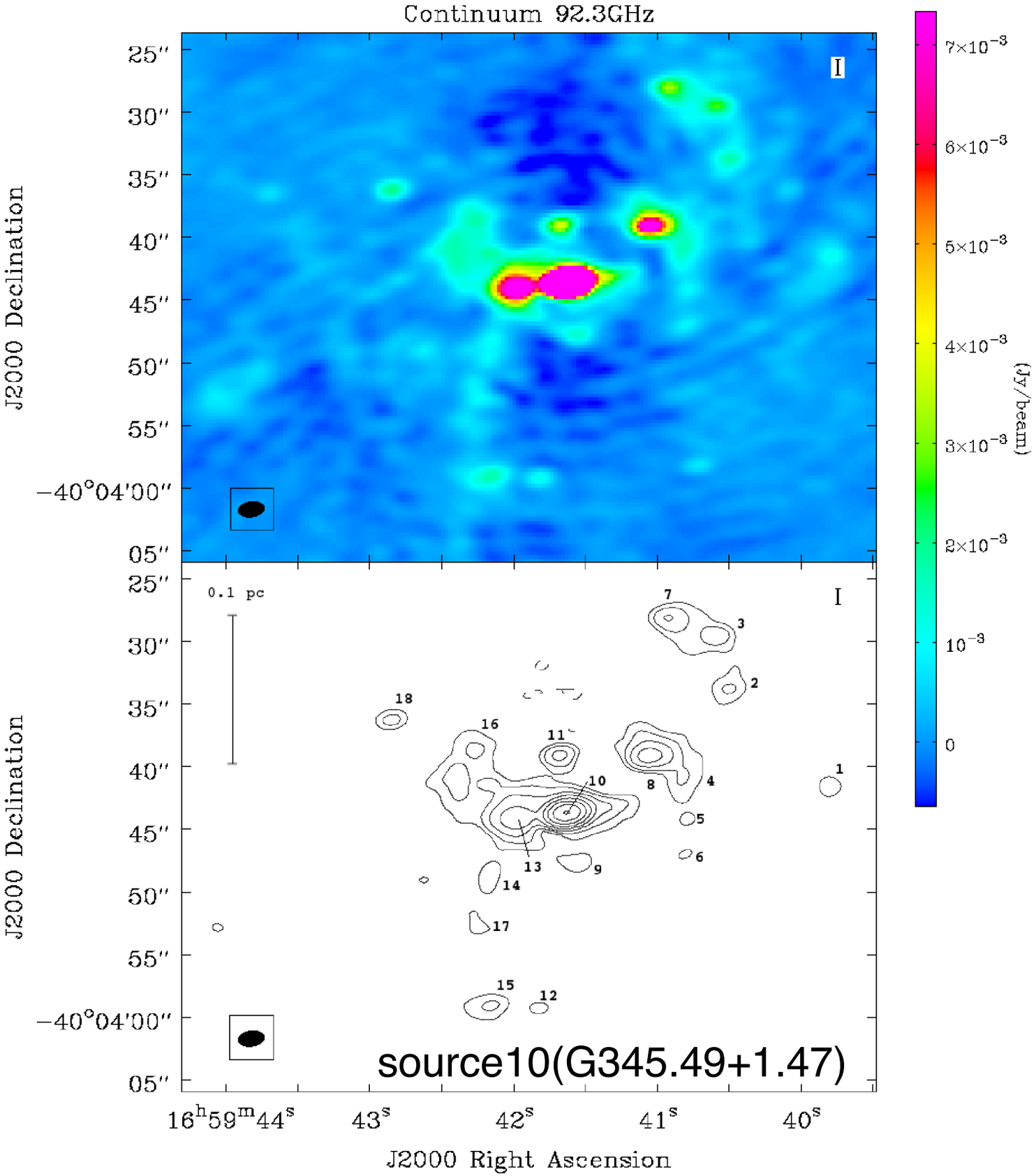

Fig. 1.— Continuum emission detected at 92.3 GHz toward IRAS 16562−3959. *Bottom panel:* Contours shown correspond to $-15, 15, 30, 60, 120, 250, 500, 1000$, and $2000\,\sigma$, with $\sigma = 50$ μJy beam^{-1}. σ represents the r.m.s. variations of the dynamic range limited image measured at the edge of the field. Compact sources are identified by the number given in Table 2. All sources are within the

source10からHRL

(水素再結合線)

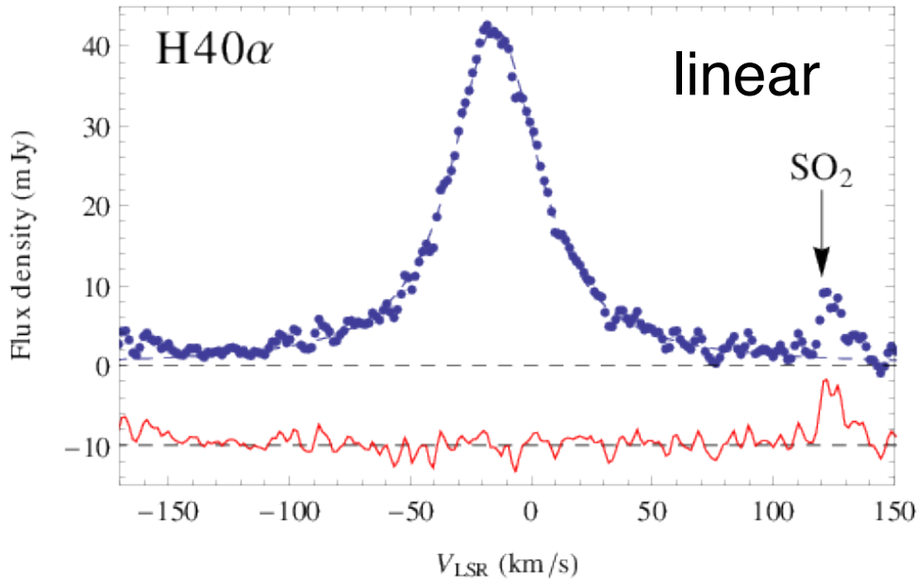

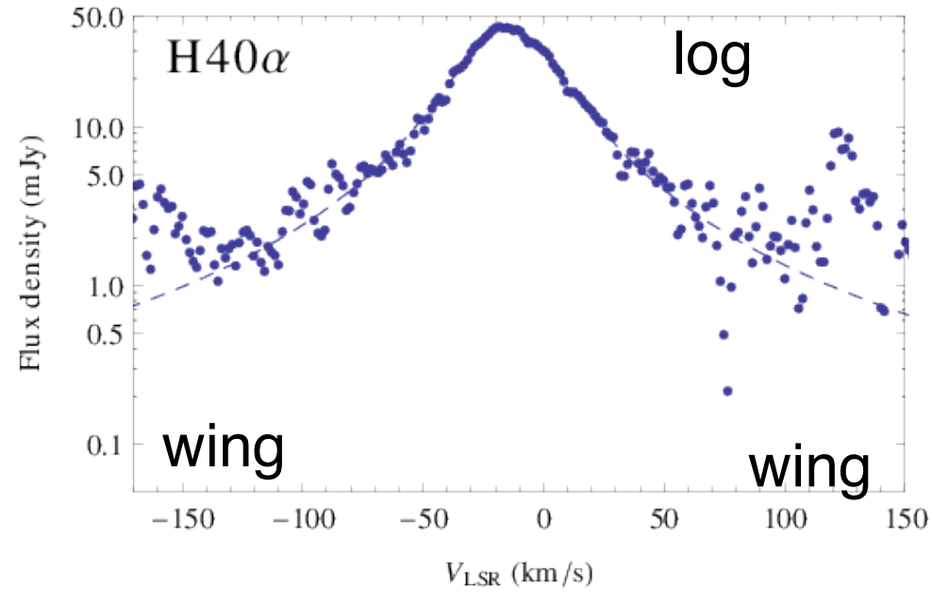

Stark効果によるブロードニング

→電子密度を求めた